MATERIALS CHEMISTRY
FRONTIERS

RESEARCH ARTICLE

View Article Online
View Journal | View Issue

Cite this: *Mater. Chem. Front.*, 2018, **2**, 1529

Folate-conjugated and pH-triggered doxorubicin and paclitaxel co-delivery micellar system for targeted anticancer drug delivery

Lijing Niu,†[a] Feiyan Zhu,†[b] Bowen Li,[a] Lingling Zhao, *[ac] Hongze Liang,[a] Yinghua Yan [a] and Hui Tan*[c]

Received 8th May 2018,
Accepted 5th June 2018

DOI: 10.1039/c8qm00217g

rsc.li/frontiers-materials

A folate-conjugated and pH-sensitive polymeric micellar system for the co-delivery of DOX and PTX was studied. A doxorubicin conjugated prodrug was synthesized *via* Schiff's base reaction. Subsequently, folate was grafted onto the prodrug and PTX was encapsulated. Sustained drug release of both DOX and PTX from the polymeric micelles was observed and the release rate could be accelerated by decreasing the media pH. A cellular uptake assay revealed that the polymeric micelles were internalized in the cytoplasm *via* endocytosis by SW1353 cells, and the cellular uptake was enhanced for the folate-conjugated micelles due to an active FR-mediated endocytosis pathway, showing stronger red fluorescence compared to that of non-folate micelles. The *in vitro* anticancer efficiency of the polymeric micellar system was evaluated using a cytotoxicity assay by incubating different drug formulations with the SW1353 cells. Both free drugs and micellar formulations displayed inhibition of cell growth at different levels, while the folate-conjugated dual-drug loaded polymeric micelles (Folate–Oxd–DOX/PTX) displayed a much lower IC_{50} value than other drug formulations, indicating a desirable *in vitro* anticancer efficiency due to the synergistic effect of co-delivery and active targeting. Thus, the polymeric micellar system is a promising platform for targeted cancer chemotherapy.

Introduction

Chemotherapy accompanied by radiotherapy and surgery is the principal cancer therapeutic method in the clinic at present. However, the widely used clinical chemotherapeutic drugs such as doxorubicin (DOX), paclitaxel (PTX), cisplatin and so on, are far from perfect because of their undesirable side effects and low bioavailability owing to their lack of targeting ability.[1,2] Furthermore, the development of multidrug resistance (MDR) can even lead to chemotherapy failure.[3,4] Over the past few decades, various nano-scaled drug delivery systems including nanoparticles, polymeric micelles, liposomes and prodrugs,[5–8] have been developed to solve the existing problems on the basis of the intrinsic EPR effect of solid tumors.[9,10] Smart drug carriers, which can respond to environmental stimuli including pH, temperature, light, biomolecules and so on, have attracted wide interest in anticancer drug delivery due to the subtle differences in the physiological microenvironments between tumor and normal tissues. For example, the extracellular microenvironment of tumor tissue is much more acidic (pH ~ 6.8) than normal tissue because of the more active aerobic glycolysis at tumor sites.[11,12] Accordingly, plenty of pH-responsive platforms such as liposomes,[13] nanogels,[14] micelles,[15] and conjugates[16] have been applied to control the drug release at tumor tissue. pH-responsive platforms based on acid-sensitive covalent bonds including amide,[17] acetal,[18] hydrazine,[19] imine,[20,21] and boronate bonds[22] as well as charged polymers[23] have been studied. It has been reported that many malignant tissue cells consistently express high levels of specific receptors such as folate receptors (FR-a, FR),[24–26] thus folate could be applied to modify the surface of drug carriers in order to enhance the cellular uptake *via* the route of FR-mediated endocytosis due to the high binding affinity between folate and FR.

In addition, co-delivery systems, which can load different drugs simultaneously, have drawn great attention for combination chemotherapy in pharmaceutical research. Co-delivery systems have become promising strategies to improve cancer treatment and have been proposed to overcome undesirable toxicity and other side effects, such as reversing multidrug resistance (MDR),[11,27,28] reducing the dosage of each agent

[a] *Ningbo University, School of Materials Science and Chemical Engineering, Ningbo, 315211, China. E-mail: zhaolingling@nbu.edu.cn*
[b] *Shenzhen Key Laboratory of Tissue Engineering, Shenzhen Laboratory of Digital Orthopaedic Engineering, The First Hospital Affiliated to Shenzhen University, Shenzhen, 518035, China*
[c] *The First Affiliated Hospital of Shenzhen University, Health Science Center, Shenzhen, 518035, China. E-mail: huitan@email.szu.edu.cn*
† These authors contributed equally to this work.

and achieving a synergistic therapeutic effect.[29,30] Currently, DOX and PTX are commonly prescribed chemotherapeutic agents for various malignancies in the clinic due to their excellent anticancer efficiency.[31] DOX is an anthracycline antibiotic, which interacts with DNA through intercalation and results in the inhibition of macromolecular biosynthesis.[6,32] Meanwhile the application of DOX is associated with a series of physiological drawbacks such as systematic toxicity, especially cardiotoxicity, lack of stability, and so forth.[33] PTX usually acts as a microtubule stabilizer and stabilizes the polymerization of cellular microtubules in the G2 mitotic phase to prevent cell division.[34,35] However, the clinical application of PTX is restricted due to its poor solubility. The current clinical PTX formulations based on Cremophor EL and ethanol (Taxol) to improve the solubility of PTX were compromised by hypersensitivity reactions.[18,36] Some studies have shown that the combination of DOX and PTX has shown an increased tumor regression rate and enhanced patient survival rate compared to single-agent therapy.[5,6,37] However, the co-delivery of DOX and PTX remains a challenge due to the distinct solubility characteristics of the two drugs. There are several methods reported to combine DOX and PTX in a single drug carrier. For instance, injectable hydrogels with hydrophobic microdomains[37] and polymersomes with an apparent bilayered lamellar structure[5] were developed to co-encapsulate DOX and PTX. High-pressure homogenization and evaporation technology was utilized to fabricate DOX and PTX co-bound nanoparticles with good liver targetability.[38]

Herein, in this work, a co-delivery system for DOX and PTX was well-designed and synthesized based on a folate-conjugated and pH-sensitive polymeric micellar system. Dextran, a natural hydrophilic polysaccharide, was selected as a starting material due to its fine biodegradability and biocompatibility.[7,16] Oxidized dextran (Oxd) obtained from the oxidization of dextran contains a large number of hydroxyl and aldehyde groups, offering adequate binding sites for both drug molecules (*e.g.* DOX) and targeting ligands (*e.g.* folate). Oxd–DOX conjugate prodrugs were prepared *via* a pH-sensitive Schiff's base linkage between the amino group of DOX and the aldehyde group of Oxd. The prodrugs are amphiphilic and could self-assemble in aqueous solution to improve the solubility of PTX, forming a polymeric micellar system co-encapsulating DOX and PTX for combination chemotherapy. Folate was anchored to the prodrug conjugates as a targeting ligand to enhance the tumor targetability of the micellar system. The physicochemical properties, release profile, cellular uptake and *in vitro* anticancer efficiency of the polymeric micelles were evaluated in the present work.

Experimental

Materials

Oxidized dextran (Oxd) (M_W 30.8 kDa, oxidation degree 20.8%) was synthesized according to our previous work.[39] Doxorubicin hydrochloride (DOX) was purchased from Beijing Huafeng United Technology, China. PTX was purchased from Xi'an Sanjiang Bioengineering Co. Ltd, China. Folate was purchased from Aladdin Industrial Corporation, China. *N*-Hydroxysuccinimide (NHS) was purchased from Quzhou Xinteng Chemical, China. 1-(3-Dimethylaminopropyl)-3-ethyl carbodiimide hydrochloride (EDC·HCl) was purchased from Sigma Aldrich (St. Louis, China). Distilled and deionized water was used in all experiments.

Synthesis of DOX conjugated Oxd (Oxd–DOX)

The Oxd–DOX prodrug was synthesized *via* Schiff's base reaction between the amino group of DOX and the aldehyde group of Oxd. Briefly, 800 mg of Oxd was dissolved in 50 mL of DMSO to form a uniform solution. 100 mg of DOX was dissolved in 20 mL of DMSO, and then 15 μL of triethylamine was added to remove the hydrochloric acid. The two solutions were mixed and stirred at room temperature for 24 h in the dark. The resultant solution was transferred to dialysis tubing (MWCO 12 kDa) and dialyzed against $NaHCO_3$ solution (pH 7–8) with six changes every 4 h, then against distilled water with four changes over 12 h at room temperature. The dialysate was freeze-dried to harvest the dark red products (yield, 83%).

Synthesis of folate modified Oxd–DOX (Folate–Oxd–DOX)

85 mg of folate, 44 mg of NHS, and 44 mg of EDC·HCl were dissolved in DMSO and the mixture was stirred at room temperature for 30 min. To this, 85 mg of Oxd–DOX dissolved in 24 mL of DMSO was added and stirred for 24 h in the dark. Then, the mixture was transferred to dialysis tubing (MWCO 12 kDa) and dialyzed against $NaHCO_3$ solution (pH 7–8) with six changes every 4 h, then against distilled water with four changes over 12 h at room temperature. The dialysate was freeze-dried to harvest the brown powder-like products (yield, 87%). The content of folate in Folate–Oxd–DOX was measured spectrophotometrically at a wavelength of 360 nm in DMSO using the calibration curve obtained from folate with different concentrations.

Measurement of critical micelle concentration (CMC)

The CMC of Oxd–DOX and Folate–Oxd–DOX was determined using the pyrene 1 : 3 ratio method. There are five peaks (near 372, 379, 383, 394 and 480 nm) in the fluorescence emission spectrum of the pyrene solution, and the characteristic dependence of the fluorescence vibrational fine structure could be applied to determine the CMC in micellar systems.[40,41] The pyrene 1 : 3 ratio value corresponds to a polar environment below the CMC and decreases rapidly around the CMC, indicating that the pyrene is sensing a more hydrophobic environment; then it reaches a roughly constant value above the CMC due to the incorporation of the pyrene probe into the hydrophobic region of the micelles.[42] The CMC value could be obtained from the inflection point in the plots of the pyrene 1 : 3 ratio against polymer concentration. The detailed process was referred from the previous work.[43] Briefly, 200 μL of pyrene solution (dissolved in acetone, 10^{-5} mol L^{-1}) was added to a series of 10 mL vials, respectively. After acetone was evaporated, 2 mL of Oxd–DOX or Folate–Oxd–DOX with various concentrations (1×10^{-6} to 0.5 mg mL^{-1}) was added to each vial. The mixture was sonicated for 30 min at room temperature and

then heated at 37 °C for 24 h to equilibrate pyrene and the micelles, and subsequently left to cool at room temperature. Fluorescence emission spectra of the sample solution were obtained at an excitation wavelength of 335 nm and an emission wavelength range from 360 to 420 nm. The excitation and emission bandwidths were both set at 5 nm. The curve of I_{372}/I_{383} against the log concentrations of Oxd–DOX or Folate–Oxd–DOX was plotted based on the pyrene emission spectra, and the CMC value was calculated by the crossover point at which I_{372}/I_{383} began to decrease rapidly.

Preparation of DOX and PTX dual-loaded polymeric micelles

15 mg of PTX was dissolved in 1 mL of methanol and then the solution was added dropwise to an Oxd–DOX or Folate–Oxd–DOX solution (30 mg in 30 mL of distilled water) under stirring. After stirring at room temperature for 4 h, the solution was transferred to dialysis tubing (MWCO 12 kDa) and dialyzed for 24 h to remove the organic solvents and free PTX. The solution was freeze-dried to obtain the DOX and PTX dual-loaded polymeric micelles. The whole procedure was performed in the dark. The products were coded as Oxd–DOX/PTX and Folate–Oxd–DOX/PTX, respectively.

The content of DOX in the polymeric micelles was determined by fluorescence spectrometry (F-4600, Hitachi factory, Japan) at a wavelength of 594 nm using the calibration curve obtained from DOX in DMSO solutions with different DOX concentrations. The excitation wavelength was 494 nm and both the excitation and emission bandwidths were set at 10 nm. The content of PTX in the polymeric micelles was quantified using reversed-phase high-performance liquid chromatography (RP-HPLC, Shimadzu, SPD-M20A, Kyoto, Japan) with a UV detector set at 227 nm. In detail, 1 mg of Oxd–DOX/PTX or Folate–Oxd–DOX/PTX was dissolved in 10 mL of a mixture solution (acetonitrile/water, 3/1, v/v). 20 μL of the sample solution was injected into an AM12S05-1546WT column (150 mm × 4.6 mm, 5.0 μm, YMC Ltd, China) and eluted with a mobile phase consisting of acetonitrile/water/methol (40/35/25, v/v/v) at a flow rate of 1 mL min^{-1}.

Characterization

^1H NMR analysis of the sample was tested in DMSO-d_6 solution using a Bruker AMX 400 MHz spectrometer. FTIR was performed on pressed polymer/KBr using a Nicolet 6700 spectrometer. Transmission electron microscopy (TEM) was carried out on a JEM-2011 microscope at an operating voltage of 200 kV. Samples were dispersed in water and dropped onto carbon-coated copper grids and then stained with 0.5 wt% phosphotungstic acid (PTA) after air-dried. The size distribution of the self-assembled polymeric micelles was tested in aqueous dispersion using a Zetasizer (Nano Series, Malvern Instruments, UK) at 25 °C. The test was repeated three times at a constant concentration of 0.1 mg mL^{-1} at the desired pH. NaOH and HCl were used to adjust the pH values of the aqueous dispersion of the samples when needed.

In vitro drug release

The *in vitro* release behavior of the DOX and PTX dual-loaded polymeric micelles was investigated in PBS media at different pH values containing 0.1% (v/v) Tween-80.[37,40] Typically, Oxd–DOX/PTX or Folate–Oxd–DOX/PTX was dispersed in PBS (0.01 M, pH 7.4) at a concentration of 1 mg mL^{-1}. Subsequently, 1 mL of the dispersion was transferred into each dialysis tubing (MWCO 12 kDa), respectively. The tubings were immersed in vials containing 10 mL of medium at the desired pH at 37 °C. Periodically, 2 mL of released medium was taken out and replenished with an equal volume of fresh medium. The amount of released DOX was detected by a fluorescence detector with an excitation wavelength at 494 nm and emission wavelength at 594 nm. The amount of released PTX was detected by HPLC at 227 nm. The released samples were diluted with three equal volumes of acetonitrile, and 20 μL of sample was injected into an AM12S05-1546WT column (150 mm × 4.6 mm, 5.0 μm, YMC Ltd, China) and eluted with a mobile phase consisting of acetonitrile/water/methol (40/35/25, v/v/v) at a flow rate of 1 mL min^{-1}. The release experiments were performed in triplicate and the results were presented as the average data with standard deviations.

Cellular uptake

The polymeric micelles were incubated with SW1353 chondrosarcoma cells to evaluate the cellular uptake behavior using confocal laser scanning microscopy (CLSM, ZEISS). The SW1353 cells were seeded onto glass dishes (35 mm diameter) at a density of 1×10^4 cells per well using Dulbecco's Modified Eagle's Medium F-12 (DMEM/F-12) supplemented with 10% fetal bovine serum and 1% penicillin–streptomycin and then incubated at 37 °C under a humidified atmosphere containing 5% CO_2 for 24 h. Then 500 μL of DOX or the DOX containing polymeric micelles in DMEM/F-12 (the equivalent concentration of DOX in each sample was 50 μg mL^{-1}) were added to each of the wells, respectively. The culture medium was removed and the dishes were rinsed with PBS three times after 3 h of incubation at 37 °C. The cell nucleus was stained with DAPI for 20 min and then washed with PBS. To further confirm that the folate-conjugated polymeric micelles were taken up through active FR-mediated endocytosis, the SW1353 cells were incubated with an excess of free folate (2 mM) for 4 h. Subsequently, DOX or the DOX containing polymeric micelles were added and the other conditions were kept consistent. CLSM images of the cells were observed using an LSM 800 confocal laser scanning microscope (ZEISS, Germany). The excitation wavelength was 405 and 488 nm and the emission wavelength range was 425–475 nm and 500–580 nm for DAPI and DOX, respectively.

In vitro anticancer efficiency

The *in vitro* anticancer efficiency of the different drug formulations against SW1353 cells was evaluated using the CCK-8 assay. The cells were seeded onto 96-well plates at a density of 1×10^4 cells per mL in 100 μL of DMEM/F-12. After 24 h incubation, the culture medium was removed and replaced with 100 μL of medium containing drug formulations at different concentrations (from 0.001 to 500 μg mL^{-1}) in DMEM/F-12. The culture medium was removed after 24 h incubation, and the

wells were rinsed with PBS thrice. Subsequently, 100 μL of DMEM/F-12 containing 10 μL of CCK-8 assay solution was added to each well of the plate for another 2 h incubation. The absorbance at 450 nm of each well was detected using a microplate reader (Thermo MULTISKAN G0), and the cell viability was calculated through the following formula.

$$\text{Cell viability (\%)} = I_s/I_c \times 100$$

where I_s is the OD value of the cells incubated with different drugs formulations and I_c is the OD value of the cells incubated with DMEM/F-12 only. The IC_{50} (half maximal inhibitory concentration) of the drugs and polymeric micelles was calculated using SPSS software (n = 4).

Results and discussion

Synthesis of Oxd–DOX and Folate–Oxd–DOX

The synthesis of Oxd–DOX and Folate–Oxd–DOX is illustrated in Scheme 1a. The conjugation of DOX and folate to Oxd was accomplished through Schiff's base reaction and esterification, respectively. The structure of the synthesized Oxd–DOX and Folate–Oxd–DOX was confirmed by ^{1}H NMR and FTIR. As shown in Fig. 1a, the broad absorption band between 3100 and 3650 cm^{-1} was owing to the O–H stretch, and the peaks at 2933 and 2845 cm^{-1} were attributed to the presence of C–H stretching. The peaks at 1082 and 1010 cm^{-1} indicated the presence of C–O of DOX and Oxd, respectively. Compared to Oxd, the absorption band at 1600 cm^{-1} in the spectrum of Oxd–DOX was assigned to the benzene skeleton vibration ($\nu_{C=C}$), and the appearance of the peak at ~1375 cm^{-1} was attributed to the symmetric bending vibration of C–H in the methyl group, testifying the conjugation of DOX to Oxd. In the FTIR spectrum of Folate–Oxd–DOX (Fig. 1b), the absorption peak at 2835 cm^{-1}, which was attributed to the stretching vibration of –CH_2, showed a shift to a lower wave number, testifying the presence of the –CH_2–NH– group in folate. Compared with Oxd–DOX, Folate–Oxd–DOX showed an increased peak at ~1135 cm^{-1} assigned to the stretching vibration of C–N, suggesting the conjugation of folate to Oxd–DOX. ^{1}H NMR was also performed to determine the chemical structure of Oxd–DOX and Folate–Oxd–DOX. As shown in Fig. 2a, the broad peak at ~3.6 ppm (overlapping multiplet superimposed on the H_2O peak of DMSO-d_6) in the Oxd spectrum was assigned to the protons of C_b–C_f in the Oxd unit. The peak with a low intensity at 9.7 ppm belongs to the aldehyde protons due to the formation of hemiacetals.[44] Oxd–DOX was confirmed by the disappearance of the aldehyde proton signals at 9.7 ppm, compared with Oxd, as well as the presence of new signals at 7.6 and 7.9 ppm belonging to the aromatic protons of DOX[7,45] (Fig. 2b). The peaks appeared at 6.8, and 8.9 ppm in Folate–Oxd–DOX were assigned to protons of the benzene and pteridine rings in folate[32,43] (Fig. 2c), suggesting the successful conjugation of folate to Oxd–DOX. The amount of DOX and folate in Oxd–DOX and

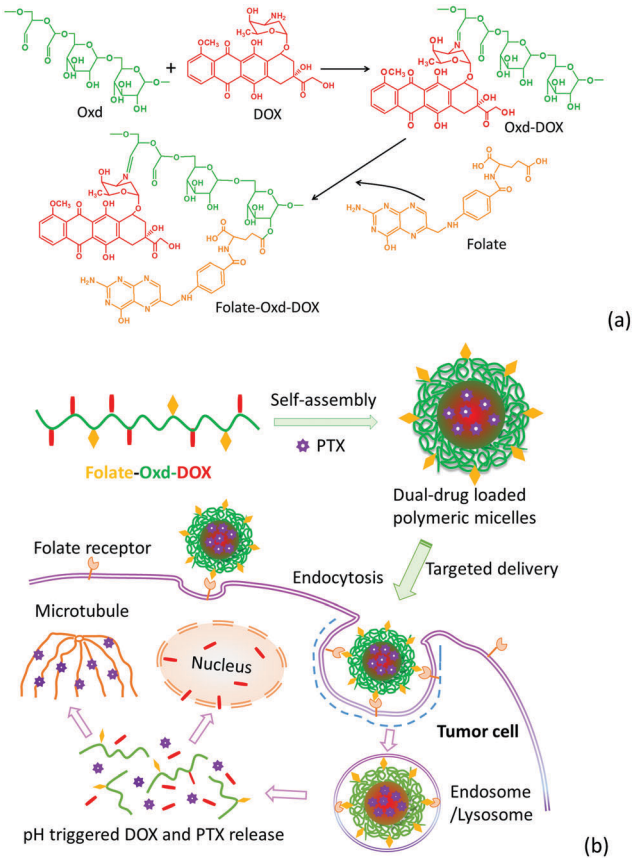

Scheme 1 Illustrative synthesis of Folate–Oxd–DOX (a). The formation of the dual-drug loaded micelles, and the cellular uptake of the micelles by tumor cells and drug release in response to the characteristic stimuli of tumor tissues and intracellular microenvironments (b).

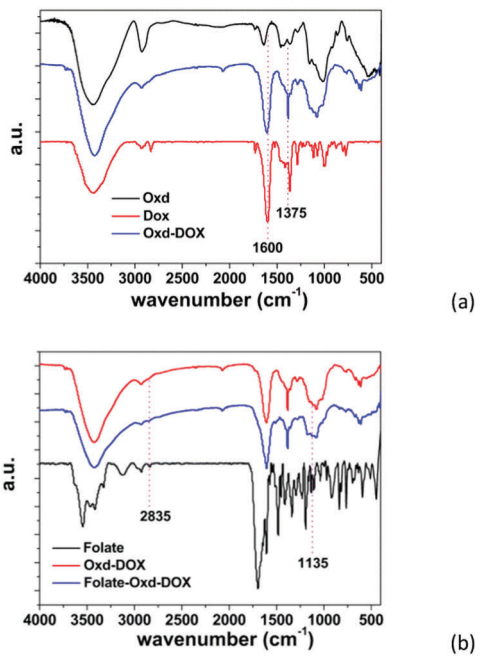

Fig. 1 FTIR spectra of Oxd–DOX (a) and Folate–Oxd–DOX (b).

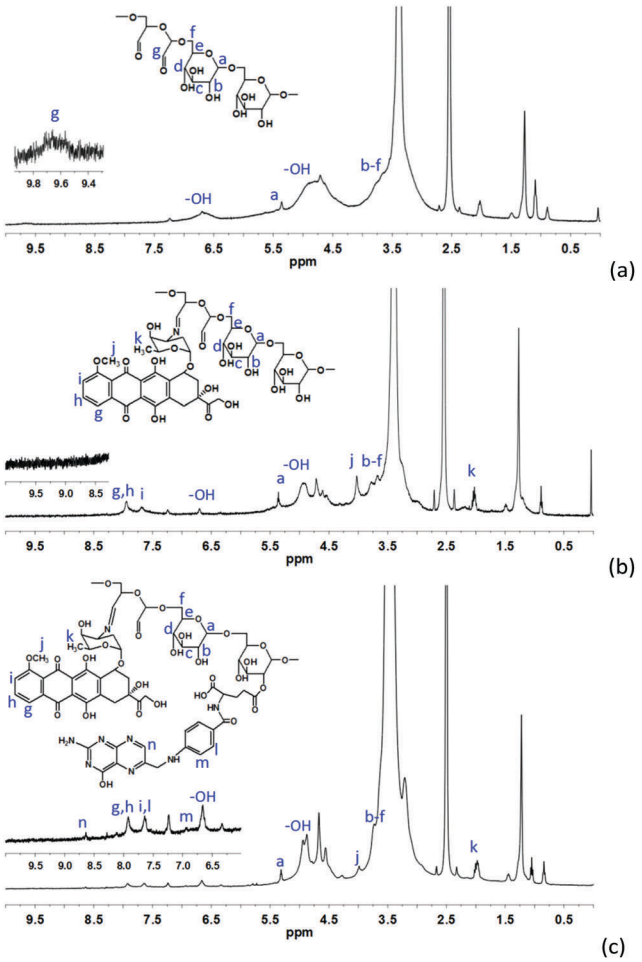

Fig. 2 ^{1}H NMR spectra of Oxd (a), Oxd–DOX (b) and Folate–Oxd–DOX (c).

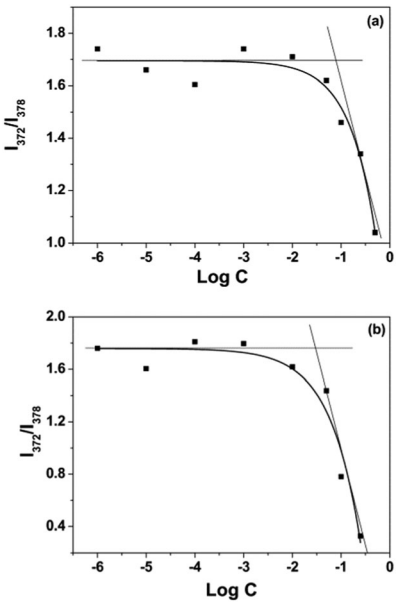

Fig. 3 The intensity ratio (I_{372}/I_{383}) of the pyrene emission *versus* the log concentration of Oxd–DOX (a) and Folate–Oxd–DOX (b).

Folate–Oxd–DOX was determined by fluorescence and UV-Vis spectrometry, respectively, and the result is shown in Table 1.

Characterization of the polymeric micelles

Oxd–DOX and Folate–Oxd–DOX can self-assemble to form polymeric micelles in solution due to their amphiphilic nature. The CMC of Oxd–DOX and Folate–Oxd–DOX was determined by fluorescence spectrometry using pyrene as a probe. As shown in Fig. 3, the changes in the fluorescence intensity ratio of I_{372}/I_{383} were small or negligible when the concentration of Oxd–DOX and Folate–Oxd–DOX was below the CMC, whereas a remarkable decrease of I_{372}/I_{383} was observed as the concentration increased. The CMC value was calculated from the crossover point based on the I_{372}/I_{383}–log C curve. The CMC of Oxd–DOX and Folate–Oxd–DOX is 0.066 and 0.030 mg mL^{-1}, respectively (Table 1). The morphology of the assembled polymeric micelles was spherical aggregates, as shown in the TEM images (Fig. 4). The sizes of the polymeric micelles measured by DLS were 203 ± 20 and 311 ± 16 nm for Oxd–DOX and Folate–Oxd–DOX, respectively, which was consistent with the TEM observation.

PTX was employed as a hydrophobic anticancer model drug to construct the dual-drug loaded polymeric micelles and encapsulated in the hydrophobic domains of the micelles during the self-assembly of Oxd–DOX or Folate–Oxd–DOX. The content of PTX in the dual-drug loaded polymeric micelles was measured by HPLC, and the result is shown in Table 1. The morphologies of the dual-drug loaded polymeric micelles maintained spherical shapes similar to the non-PTX loaded polymeric micelles (Fig. 4), while the size of the polymeric micelles increased after PTX loading. As shown in Fig. 5a and b, the size of Oxd–DOX/PTX (413 ± 72 nm) increased in comparison with that of Oxd–DOX (203 ± 20 nm), and the hydrodynamic

Table 1 The content of DOX, folate and PTX in the polymeric micelles, the CMC, the particle size and the IC_{50} value of the SW1353 cells for the polymeric micelles

Sample	Content of DOX[a] (wt%)	Content of folate[b] (wt%)	Content of PTX[c] (wt%)	DLE (%, PTX)	CMC[d] (mg mL^{-1})	Particle size[e] (nm)	IC_{50}[f] (μg mL^{-1})
Oxd–DOX	22.5	—	—	—	0.066	203 ± 20	18.1
Oxd–DOX/PTX	13.6	—	55.6	84.4	—	413 ± 72	6.2
Folate–Oxd–DOX	17.8	45.8	—	—	0.030	311 ± 16	14.1
Folate–Oxd–DOX/PTX	8.2	9.7	37.0	66.6	—	455 ± 36	0.925

[a] Determined by fluorescence spectrometry. [b] Determined by UV-Vis spectrometry. [c] Determined by HPLC. [d] Determined by the I_{372}/I_{383} ratio (I_1/I_3) of pyrene emission fluorescence as a function of polymer concentration. [e] Mean value measured using DLS. [f] Calculated based on the cell viability *versus* the polymeric micelle concentration using SPSS software.

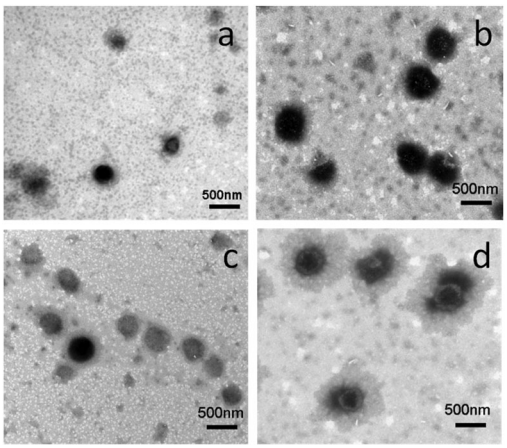

Fig. 4 TEM images of the polymeric micelles at pH 7.4. Oxd–DOX (a), Oxd–DOX/PTX (b), Folate–Oxd–DOX (c) and Folate–Oxd–DOX/PTX (d).

diameter of Folate–Oxd–DOX/PTX increased from 311 ± 16 nm (Folate–Oxd–DOX) to 455 ± 36 nm, tested by DLS. In addition, the relative stability of the micelles was also confirmed. The polymeric micelles were incubated in PBS for 68 h, and the sizes of the micelles were measured by DLS at intervals. As shown in Fig. 5c, the sizes of Oxd–DOX and Oxd–DOX/PTX incubated in PBS (pH 7.4) at room temperature were nearly uniform within 68 h, suggesting good stability of the micelles under normal physiological conditions. The size of Folate–Oxd–DOX showed a small fluctuation within 48 h and had a slight decrease at 68 h. The size change of Folate–Oxd–DOX/PTX incubated in PBS was small within 24 h, while the size reduced by ~140 nm at 68 h, probably due to the release of DOX from the micelles at pH 7.4 during the incubation time, as shown in the *in vitro* drug release assay (Fig. 7c).

DOX was conjugated to Oxd *via* low pH labile bonds. Hence, the polymeric micelles were supposed to be pH responsive due to the hydrolysis of Schiff's base under acidic conditions, and the size changes depending on the pH value were observed in this study. As shown in Fig. 6a, the size of the Oxd–DOX micelles was 203 ± 20 nm at pH 7.4 and increased to 263 ± 13 and 337 ± 19 nm when the pH decreased to 6.5 and 5.0, respectively, verified by DLS measurements. The folate–Oxd–DOX micelles displayed a similar pH dependence in size distribution, and the size increased to 380 ± 8 and 688 ± 120 nm at pH 6.5 and 5.0, respectively, from 311 ± 16 nm at pH 7.4 (Fig. 6b). Since Schiff's base is labile under acidic conditions, parts of the Schiff's base in the Oxd–DOX and Folate–Oxd–DOX conjugates would hydrolyze at acidic pH, thus altering the hydrophobic and hydrophilic performance of the conjugates, resulting in the swelling of the polymeric micelles and increasing the micellar sizes. The acidic pH sensitivity of the polymeric micelles is favorable for the targeted delivery of the anticancer drugs in tumor treatment because of the low pH in tumor tissues.[46]

In vitro drug release

The *in vitro* drug release behavior of the dual-drug loaded micelles was investigated in PBS containing 0.1% (v/v) Tween-80 at

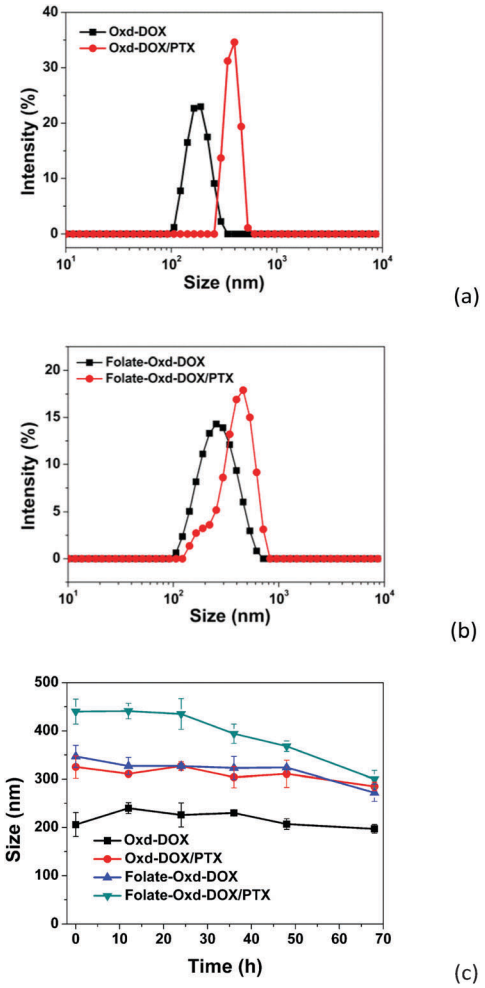

Fig. 5 Size distribution of Oxd–DOX (a) and Folate–Oxd–DOX (b) before and after PTX loading, and size changes of Oxd–DOX, Oxd–DOX/PTX, Folate–Oxd–DOX and Folate–Oxd–DOX/PTX in PBS at pH 7.4 at room temperature, with increasing time (c).

different pH values at 37 °C, and the results are plotted in Fig. 7. The sustained release of both DOX and PTX without obvious initial burst release was observed for both Oxd–DOX/PTX and Folate–Oxd–DOX/PTX, and the release of the two drugs could be accelerated by decreasing the media pH. The release rate of DOX was much faster than that of PTX and obviously influenced by the pH change. As plotted in Fig. 7a, the DOX cumulative release from Oxd–DOX/PTX was 32% at physiological pH (7.4) at day 6. Decreasing the media pH to 6.5 and 5.0 resulted in the increase of DOX release to 39 and 57%, respectively. Comparably, the pH dependence of the PTX release from Oxd–DOX/PTX was relatively minor due to its poor solubility in the media. The PTX cumulative release was 4.2, 5.1 and 6.8% at pH 7.4, 6.5 and 5.0, respectively, at day 6 (Fig. 7b). The DOX and PTX release from Folate–Oxd–DOX/PTX was faster than that of Oxd–DOX/PTX and displayed a similar trend of pH-triggered release. As shown in Fig. 7c, DOX cumulative release was 49% at physiological pH (7.4) at day 3, and increased to 60 and 94% at pH 6.5 and 5.0, respectively. The PTX release rate is relatively slow as well and the cumulative release is 4.2, 5.5 and 7.1% at pH 7.4, 6.5 and 5.0,

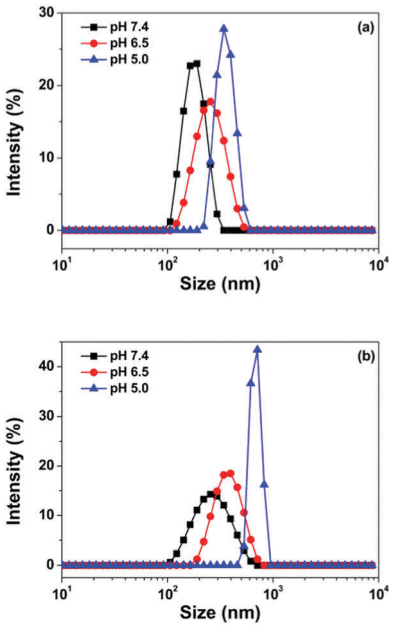

Fig. 6 The size distribution of Oxd–DOX (a) and Folate–Oxd–DOX (b) at different pH values.

respectively, at day 3 (Fig. 7d). Since DOX was covalently linked to Oxd through the pH-sensitive imine bond, the accelerated release of DOX by decreasing the media pH from 7.4 to 6.5 and 5.0 was due to the hydrolysis of the imine linkage in the micelles because Schiff's base was stable at physiological pH and labile at acidic pH.[39] For the low pH microenvironment in tumor tissue, the accelerated release of DOX and PTX from the dual-drug loaded micelles should be beneficial for their application in tumor therapy.[47] Studies also showed that the difference in the release kinetics of DOX and PTX was important for tumor treatment, because in the initial stage, more DOX released from the dual drug loaded carriers to cause the inhibition in tumor size, whereas the PTX release was kept for a longer period to improve the treatment in the later stage.[37]

Cellular uptake

The *in vitro* cellular uptake behavior of the polymeric micelles was evaluated by CLSM. The results displayed that both the free DOX and polymeric micelles could be taken up by the cells, and the red fluorescence of DOX could be observed in the cells for all the experimental groups. As shown in Fig. 8, strong red fluorescence, mainly accumulated at the nucleus, was observed in the SW1353 cells co-cultured with free DOX for 3 h, while the fluorescence intensity was much weaker in the cells incubated with Oxd–DOX and Oxd–DOX/PTX, and the red fluorescence was mainly originated from the cytoplasm, probably because the free DOX was diffused into the cells through the plasma membrane and intercalated with DNA to induce cell apoptosis, whereas Oxd–DOX and Oxd–DOX/PTX could only enter the cells *via* endocytosis due to their larger diameters.[7,48] Comparatively, stronger red fluorescence in the cytoplasm was observed in the cells co-cultured with the folate-conjugated polymeric micelles

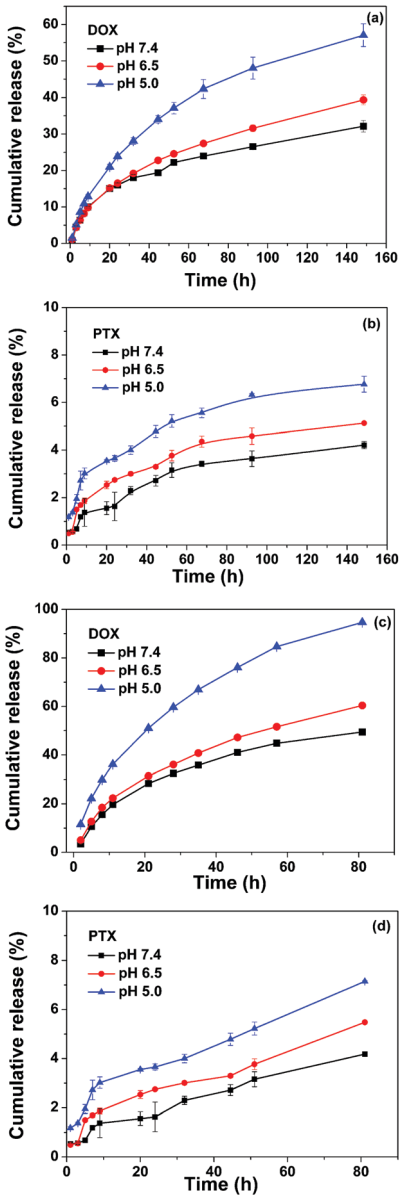

Fig. 7 Cumulative release of DOX and PTX from the dual-drug loaded micelles immersed in 10 mL of saline at different pH values. DOX release from Oxd–DOX/PTX (a), PTX release from Oxd–DOX/PTX (b), DOX release from Folate–Oxd–DOX/PTX (c) and PTX release from Folate–Oxd–DOX/PTX (d).

(Folate–Oxd–DOX and Folate–Oxd–DOX/PTX). This may be because the delivery of the folate-conjugated polymeric micelles into the cells was enhanced by folate due to the active FR-mediated endocytosis.[1,49,50] In order to demonstrate this, the SW1353 cells were co-cultured with excess folate for 4 h to interrupt the interaction between the FA-receptor in the cell membranes and the folate in the folate-conjugated polymeric micelles. Subsequently, the cells were incubated with the polymeric micelles for another 3 h. The CLSM images revealed a weak red fluorescence in the cytoplasm with no significant difference in the fluorescence intensity between the non-folate and folate-conjugated polymeric micelles, while the free DOX

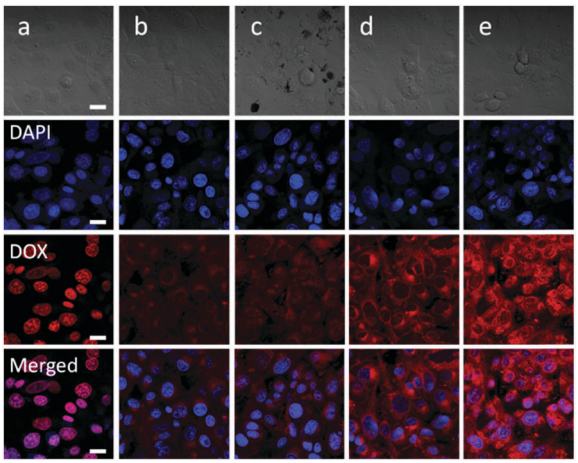

Fig. 8 CLSM images of the SW1353 cells incubated with free DOX (a), Oxd–DOX (b), Oxd–DOX/PTX (c), Folate–Oxd–DOX (d) or Folate–Oxd–DOX/PTX (e) for 3 h (the equivalent concentration of DOX in each sample was 50 μg mL^{-1}). Cell nuclei were stained with DAPI. Scale bar 20 μm.

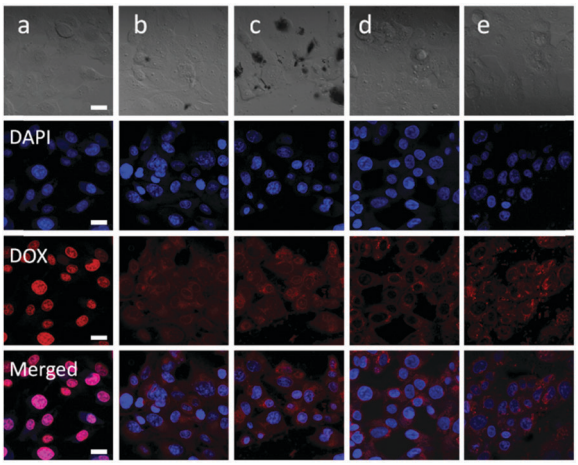

Fig. 9 CLSM images of the SW1353 cells incubated with free DOX (a), Oxd–DOX (b), Oxd–DOX/PTX (c), Folate–Oxd–DOX (d) or Folate–Oxd–DOX/PTX (e) for 3 h (the equivalent concentration of DOX in each sample was 50 mg mL^{-1}) after 4 h incubation with an excess of folate (2 mM). Cell nuclei were stained with DAPI. Scale bar 20 μm.

co-cultured cells still displayed stronger red fluorescence in the nucleus, as shown in Fig. 9. The results indicated that the internalization of the folate-conjugated polymeric micelles could be significantly inhibited by the addition of excess free folate, revealing that the folate-conjugated polymeric micelles were selectively transported through the cell membranes by an active FR-mediated endocytosis pathway due to the high level of folate receptor expression in tumor cells.

In vitro anticancer efficiency

Human chondrosarcoma cells (SW1353 cells) were used to evaluate the *in vitro* anticancer activity of the polymeric micelles, and free DOX and PTX were used as controls. As shown in Fig. 10, significant inhibition of cell growth was observed in the cells incubated with the free drugs or polymeric micelles. The IC_{50} value of Oxd–DOX was 18.1 μg mL^{-1} for the SW1353 cells, which was much higher than that of free DOX (5.0 μg mL^{-1}). This may be because free DOX could be internalized by the cells more easily and directly *via* pinocytosis and resulted in higher and nonspecific cellular uptake due to its small size and hydrophilicity,[48] while the intracellular transportation of Oxd–DOX was not as fast and efficient as the direct diffusion of free DOX. However, the effect of free DOX could be reduced with time due to the generation of drug resistance in the cells, whereas the internalization of nano- or submicrometer sized drug formulations was entered *via* endocytosis and could be enhanced by modification of targeting ligands, such as peptides, aptamers, folates and antibodies, which could facilitate the specific and efficient cellular uptake of the polymeric micelles.[51,52] This was confirmed by the cytotoxicity of Folate–Oxd–DOX against SW1353 cells, and the IC_{50} value calculated for Folate–Oxd–DOX based on Fig. 10 was 14.1 μg mL^{-1}, which was lower than that of the non-folate micelles (18.1 μg mL^{-1} for Oxd–DOX). The result was in agreement with that of the cellular uptake, wherein the cellular uptake of the folate-conjugated micelles (Folate–Oxd–DOX) was much more efficient than that of the non-folate micelles

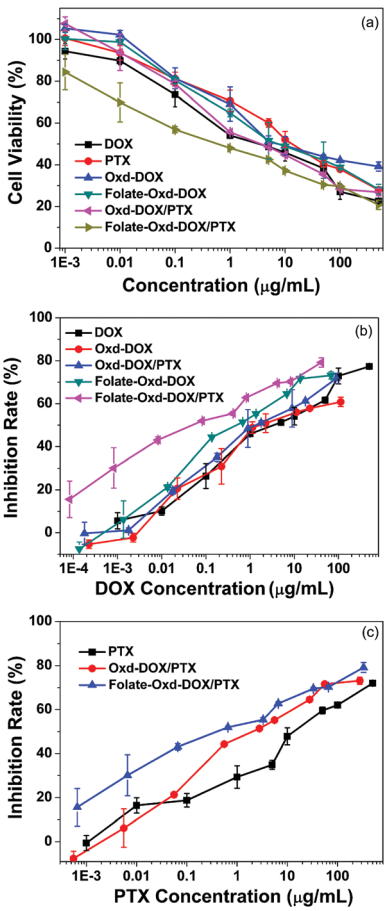

Fig. 10 Cell viability of free DOX, PTX and polymeric micelles as a function of concentration (a), and the cell growth inhibition rate of different formulations containing DOX (b) and PTX (c) against SW1353 cells. The cells were incubated with different drug formulations for 24 h.

(Oxd–DOX) *via* an active FR-mediated endocytosis pathway. Co-delivery is another strategy applied to overcome the undesirable toxicity and reverse the multidrug resistance (MDR),[11,28] thus PTX was employed as a second drug to construct the dual-drug loaded polymeric micelles. The result showed that the IC_{50} value of Oxd–DOX/PTX against the SW1353 cells was 6.2 μg mL^{-1}, which was lower than that of the micelles containing only DOX (18.1 μg mL^{-1} for Oxd–DOX) and free PTX (17.7 μg mL^{-1}), revealing the higher anticancer efficiency of the dual-drug loaded polymeric micelles. It was worth noting that the folate-conjugated and dual-drug loaded micelles (Folate–Oxd–DOX/PTX) gained notable cytotoxicity in the *in vitro* anticancer efficiency test, and the IC_{50} value of Folate–Oxd–DOX/PTX against the SW1353 cells was 0.925 μg mL^{-1}, which was much lower than that of free DOX or PTX and other polymeric micelles. This may be caused by the synergistic effect of the co-delivery of DOX and PTX, as well as the folate-mediated active targeting. Thus, the folate-conjugated and dual-drug loaded polymeric micelles have promising potential in targeted drug delivery for anticancer therapy.

Conclusion

We developed an active targeting and pH-sensitive polymeric micellar system for the co-delivery of DOX and PTX. Doxorubicin conjugated prodrugs were synthesized *via* pH-sensitive Schiff's base linkage. Subsequently, folate was grafted onto the prodrug and PTX was encapsulated in the hydrophobic domains of the polymeric micelles. Both DOX and PTX could be released from the dual-drug loaded polymeric micelles and the release rate was accelerated under weak acidic conditions. The cellular uptake and *in vitro* anticancer efficiency of the polymeric micelle system were evaluated by incubating different drug formulations with the SW1353 cells. The result displayed that the polymeric micelles were internalized in the cytoplasm *via* endocytosis, and the cellular uptake was enhanced by folate modification, showing stronger red fluorescence compared to that of non-folate micelles. The co-delivery of DOX and PTX, as well as the folate modification of the polymeric micelles, displayed a much lower IC_{50} value than that of the free drugs, and the one-drug loaded and non-folate micelles, suggesting a desirable *in vitro* anticancer efficiency due to the synergistic effect of active targeting and drug co-delivery. Hence, the folate-conjugated and dual-drug loaded polymeric micelle system appears to be a promising platform for anticancer therapy.

Conflicts of interest

There are no conflicts to declare.

Acknowledgements

We acknowledge financial support from the National Natural Science Foundation of China (51403108 and 51773119), the K. C. Wong Magna Fund at Ningbo University, the Ningbo Municipal Natural Science Foundation (2016A610049), the Science Technology Innovation Commission of Shenzhen Municipality (JCYJ20170817171930009 and JCYJ20170306093157182), and the Medical research foundation of Guangdong province (A2018116).

References

1 J. Guan, Z. Zhou, M. Chen, H. Li, D. Tong, J. Yang, J. Yao and Z. Zhang, *Acta Biomater.*, 2017, **60**, 244.
2 C. E. Ashley, E. C. Carnes, G. K. Phillips, D. Padilla, P. N. Durfee, P. A. Brown, T. N. Hanna, J. W. Liu, B. Phillips and M. B. Carter, *Nat. Mater.*, 2011, **10**, 389.
3 R. Li and Y. Xie, *J. Controlled Release*, 2017, **251**, 49.
4 Y. Yu, Z. Zhang, Y. Wang, H. Zhu, F. Li, Y. Shen and S. Guo, *Acta Biomater.*, 2017, **59**, 170.
5 D. Zhu, S. Wu, C. Hu, Z. Chen, H. Wang, F. Fan, Y. Qin, C. Wang, H. Sun and X. Leng, *Acta Biomater.*, 2017, **58**, 399.
6 Y. Ma, X. Fan and L. Li, *Carbohydr. Polym.*, 2017, **137**, 19.
7 X. Feng, D. Li, J. Han, X. Zhuang and J. Ding, *Mater. Sci. Eng., C*, 2017, **76**, 1121.
8 L. Liao, J. Liu, E. C. Dreaden, S. W. Morton, K. E. Shopsowitz, P. T. Hammond and J. A. Johnson, *J. Am. Chem. Soc.*, 2014, **136**, 5896.
9 H. Maeda, H. Nakamura and J. Fang, *Adv. Drug Delivery Rev.*, 2013, **65**, 71.
10 V. Torchilin, *Adv. Drug Delivery Rev.*, 2011, **63**, 131.
11 X. Zhao, Q. Chen, Y. Li, H. Tang, W. Liu and X. Yang, *Eur. J. Pharm. Biopharm.*, 2015, **93**, 27.
12 S. Lim, C. Li, W. Xia, H. Lee, S. Chang, J. Shen, J. L. Hsu and D. Raftery, *Cancer Res.*, 2016, **76**, 1284.
13 Y. Zhao, W. Ren, T. Zhong, S. Zhang, D. Huang, Y. Guo, X. Yao, C. Wang, W. Zhang and X. Zhang, *J. Controlled Release*, 2016, **222**, 56.
14 S. Wang, H. Wang, Z. Liu, L. Wang, X. Wang, L. Su and J. Chang, *Nanoscale*, 2014, **6**, 7635.
15 D. Sun, J. Ding, C. Xiao, J. Chen, X. Zhuang and X. Chen, *ACS Appl. Mater. Interfaces*, 2014, **6**, 21202.
16 D. Li, J. Han, J. Ding, L. Chen and X. Chen, *Carbohydr. Polym.*, 2017, **161**, 33.
17 J. Ding, F. Shi, C. Xiao, X. Zhuang, C. He and X. Chen, *J. Controlled Release*, 2013, **172**, e40.
18 Y. Gu, Y. Zhong, F. Meng, R. Cheng, C. Deng and Z. Zhong, *Biomacromolecules*, 2013, **14**, 2772.
19 Y. Bae, S. Fukushima, A. Harada and K. Kataoka, *Angew. Chem., Int. Ed.*, 2003, **42**, 4640.
20 D. Li, J. Ding, X. Zhuang, L. Chen and X. Chen, *J. Mater. Chem. B*, 2016, **4**, 5167.
21 D. Xiang, S. Shigdar, G. Qiao, T. Wang, A. Z. Kouzani, S. Zhou, L. Kong, Y. Li, C. W. Pu and W. Duan, *Theranostics*, 2015, **5**, 23.
22 W. Xu, J. Ding, C. Xiao, L. Li, X. Zhuang and X. Chen, *Biomaterials*, 2015, **54**, 72.
23 X. Loh, S. Ong, Y. Tung and H. Choo, *Polym. Chem.*, 2013, **4**, 2564.
24 X. Guo, C. Shi, G. Yang, J. Wang, Z. Cai and S. Zhou, *Chem. Mater.*, 2014, **26**, 4405.

25 E. Ahmed, S. W. Morton, P. T. Hammond and T. M. Swager, *Adv. Mater.*, 2013, **25**, 4504.
26 H. Dong, J. Lei, H. Ju, F. Zhi, H. Wang, W. Guo, Z. Zhu and F. Yan, *Angew. Chem., Int. Ed.*, 2012, **51**, 4607.
27 Q. Li, S. Lv, Z. Tang, M. Liu, D. Zhang, Y. Yang and X. Chen, *Int. J. Pharm.*, 2014, **471**, 412.
28 Y. Ma, D. Liu, D. Wang, Y. Wang, Q. Fu, J. K. Fallon, X. Yang, Z. He and F. Liu, *Mol. Pharmaceutics*, 2014, **11**, 2623.
29 N. Wiradharma, Y. W. Tong and Y. Y. Yang, *Biomaterials*, 2009, **30**, 3100.
30 W. Xiao, X. Chen, L. Yang, Y. Mao, Y. Wei and L. Chen, *Int. J. Pharm.*, 2010, **393**, 119.
31 T. Feng, H. Tian, C. Xu, L. Lin, Z. Lin, Z. Xie, M. H. W. Lam, H. Liang, H. Liang and X. Chen, *Eur. J. Pharm. Biopharm.*, 2014, **88**, 1086.
32 S. Hassanzadeh, Z. Feng, T. Pettersson and M. Hakkarainen, *Polymer*, 2015, **74**, 193.
33 O. Tacar, P. Sriamornsak and C. R. Dass, *J. Pharm. Pharmacol.*, 2013, **65**, 157.
34 Z. Li, S. Tan, S. Li, Q. Shen and K. Wang, *Oncol. Rep.*, 2017, **38**, 611.
35 Z. Du, S. Pan, Q. Yu, Y. Li, Y. Wen, W. Zhang, M. Feng and C. Wu, *Colloids Surf., A*, 2010, **353**, 140.
36 H. V. Gelderblom, J. Nooter and K. Sparreboom, *Eur. J. Cancer*, 2001, **37**, 1590.
37 L. Zhao, L. Zhu, F. Liu, C. Liu, D. Shan, Q. Wang, C. Zhang, J. Li, J. Liu and X. Qu, *Int. J. Pharm.*, 2011, **410**, 83.
38 L. Q. Thao, C. Lee, B. Kim, S. Lee, T. H. Kim, J. O. Kim, E. S. Lee, K. T. Oh, H. G. Choi, S. D. Yoo and Y. S. Youn, *Colloids Surf., B*, 2017, **152**, 18.
39 J. Li, W. Hu, Y. Zhang, H. Tan, X. Yan, L. Zhao and H. Liang, *J. Polym. Sci., Part A: Polym. Chem.*, 2015, **53**, 1235.
40 K. Kalyanasundaram and J. K. Thomas, *J. Am. Chem. Soc.*, 1977, **99**, 2039.
41 K. Kalyanasundaram, *Photochemistry in Microheterogeneous Systems*, Academic Press, New York, 1987.
42 J. Aguiar, P. Carpena, J. A. Molina-Bolívar and C. Carnero Ruiz, *J. Colloid Interface Sci.*, 2003, **258**, 116.
43 L. Zhao, Y. Zhang, J. Shao, H. Liang, H. Na and J. Zhu, *RSC Adv.*, 2016, **6**, 35658.
44 J. Maia, L. Ferreira, R. Carvalho, M. A. Ramos and M. H. Gil, *Polymer*, 2005, **46**, 9604.
45 Y. Wang, H. Wang, Y. Chen, X. Liu, Q. Jin and J. Ji, *Colloids Surf., B*, 2014, **121**, 189.
46 S. Dissanayake, W. A. Denny, S. Gamage and V. Sarojini, *J. Controlled Release*, 2017, **250**, 62.
47 T. Ramasamy, H. B. Ruttala, B. Gupta, B. K. Poudel, H. G. Choi, C. S. Yong and J. O. Kim, *J. Controlled Release*, 2017, **258**, 226.
48 Y. Lei, Y. Lai, Y. Li, S. Li, G. Cheng, D. Li, H. Li, B. He and Z. Gu, *Int. J. Pharm.*, 2013, **453**, 579.
49 Y. Sun, Y. Li, S. Nan, L. Zhang, H. Huang and J. Wang, *J. Colloid Interface Sci.*, 2015, **458**, 119.
50 S. Feng, H. Zhang, T. Yan, D. Huang, C. Zhi, H. Nakanishi and X. D. Gao, *Int. J. Nanomed.*, 2016, **11**, 4573.
51 S. Quader, X. Liu, Y. Chen, M. Peng, T. Chida, T. Ishii, Y. Miura, N. Nishiyama, H. Cabral and K. Kataoka, *J. Controlled Release*, 2017, **258**, 56.
52 L. Xu, Q. Bai, X. Zhang and H. Yang, *J. Controlled Release*, 2017, **252**, 73.

